Available online at www.sciencedirect.com
SCIENCE DIRECT®
Journal of Geodynamics 40 (2005) 51–72
JOURNAL OF GEODYNAMICS
http://www.elsevier.com/locate/jog

Dependence of diffusive radiative transfer on grain-size, temperature, and Fe-content: Implications for mantle processes

A.M. Hofmeister *

Department of Earth and Planetary Science, Washington University, St. Louis, MO 63130, USA

Received 29 November 2004; received in revised form 8 June 2005; accepted 13 June 2005

Abstract

Locally diffusive, radiative heat transport inside the earth is represented by an effective thermal conductivity ($k_{rad,dif}$), calculated from spectra. Previous geophysical models assumed that emissivity (ξ) equals unity, which violates local radiative equilibrium in an internally heated, grainy medium. Our new formulation accounts for ξ depending on frequency, physical scattering depending on grain-size (d), and for light lost through back-reflections at interfaces. Mantle values of $k_{rad,dif}$ are estimated from recent visible spectra of olivine combined with new IR data. The following trends hold for $k_{rad,dif}$ calculated from olivine spectra, and should be equally valid for pyroxene and spinel: (1) pressure is unimportant, (2) radiative thermal conductivity depends non-linearly on d, temperature (T), and Fe^{2+} content (X), (3) maxima occur in $k_{rad,dif}(d)$ when the grains are large enough to emit substantially, but not so large that light is strongly attenuated within a single-grain, (4) the dependence of $k_{rad,dif}$ on Fe^{2+} content parallels that with d because absorption is controlled by the product dX (Beer's law), and (5) a local minimum occurs in $k_{rad,dif}$ near 2000 K for $d > 2$ mm because at that temperature the peak position of the blackbody curve coincides with that of the strongly absorbing Fe^{2+} peak in the visible. Larger $k_{rad,dif}$ exists at lower and higher temperatures because mean free paths are long in the transmitting near-IR and UV spectral regions. As integration smooths over spectral details, the above representation based on olivine becomes increasingly accurate for other phases as grain-size decreases. For conditions expected in the transition zone, $\partial k_{rad,dif}/\partial T$ is negative, which is destabilizing [Dubuffet, F., Yuen, D.A., Rainey, E.S.G., 2002. Controlling thermal chaos in the mantle by positive feedback from radiative thermal conductivity. Nonlinear Proc. Geophys. 9, 1–13]. In the lower mantle, photon transport dominates phonon, promoting stable, weak convection. That radiative transfer is linked to chemical com-

* Tel.: +1 314 935 7440; fax: +1 314 935 7361.
E-mail address: hofmeist@levee.wustl.edu.

0264-3707/$ – see front matter
doi:10.1016/j.jog.2005.06.001

position and grain-size suggests that this process impacts planetary evolution through the non-linear feedback with rheology.

Keywords: Thermal conductivity; Radiative transport; Local diffusive approximation; Emissivity; Spectroscopy; Mantle; Grain-size; Fe content

1. Introduction

Heat is transported in electrically insulating solids by both lattice vibrations (phonons) and radiation (photons). Regardless of which mechanism operates, convection models implicitly assume that planetary heat flow occurs via diffusion by incorporating an effective thermal conductivity. Geodynamics models (e.g. Dubuffet et al., 1999, 2002; Yuen et al., 2000) have shown that thermal conductivity (k) being temperature (T) dependent profoundly influences heat transport in the earth. Effects of variable k cannot be overridden by variable viscosity, even for a large viscosity contrast (Yanagawa et al., 2005; van den Berg et al., 2004). The inferred behavior is complex and counterintuitive because the lattice ($k_{\rm lat}$) and the diffusive radiative ($k_{\rm rad,dif}$) components compete (e.g. van den Berg et al., 2001).

Quantifying $k_{\rm rad,dif}$ is needed to realistically model the hot lower mantle. This component cannot be extracted from laboratory measurements of thermal conductivity because the steep temperature gradients and small sample sizes present in experiments allow a different type of radiative transfer to occur, known as direct or boundary-to-boundary wherein light from the source warms the thermocouple with negligible participation of the sample (e.g. Lee and Kingery, 1960; Kanamori et al., 1968; Mehling et al., 1998). Instead, $k_{\rm rad,dif}$ is calculated from spectroscopic data. Grain-to-grain diffusion (Fig. 1, white arrows) of internally generated heat describes the physical process within the mantle. That radiative transfer in the mantle is diffusive, not direct, and therefore complies with the locally diffusive conditions of geodynamic models, is ascertained by estimating the effect of scattering on photon mean free path. The average grain-size in the mantle is expected to be ∼0.1–10 mm (e.g. Boyd and Meyer, 1979; Yamazaki and Karato, 2001). If a trivial amount (0.005%) of the photons are back-reflected from gain boundaries due to almost negligible mismatches of the index of refraction, then light is essentially extinguished over distances of 2–200 m. Mantle gradients are only ∼10 K/km in boundary layers such as D'', which makes in unlikely that light emitted from any given grain will reach another grain with temperature differing by 1 K. In contrast, in the laboratory photon mean free paths are ∼5 mm compared to sample dimensions of ∼5–14 mm (e.g. Gibert et al., 2005), in which case much of the light emitted by the source reaches the thermocouple without interacting with the sample (Fig. 1, black arrow). Values of $k_{\rm rad}$ inferred by assuming a form for $k_{\rm lat}$ and subtracting this from measured k values (e.g. Schatz and Simmons, 1972; Gibert et al., 2005) thus largely represent direct radiative transfer, which is not relevant to the mantle.

Although grain-size is unimportant to vibrational transport (e.g. Gibert et al., 2003), scattering from grain boundaries clearly affects the much longer mean free path of photons. Hofmeister's (1999) quantum mechanical treatment cannot be modified to account for grain-to-grain absorption, scattering, and emission of light in the grainy mantle. Instead, the present paper revises the macroscopic theory of diffusive radiative transfer, based on the attenuation of light that was developed in the engineering literature and introduced to geophysics by Clark (1957). Allowing for the frequency dependence of the absorptivity (Shankland et al., 1979) was an important advance, although most workers followed Clark (1957) by using a mean

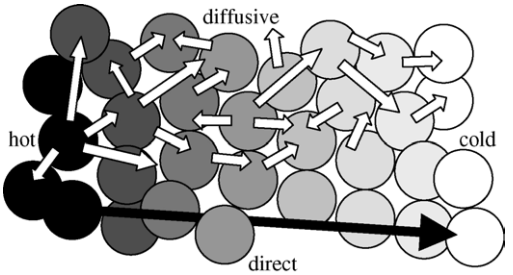

Fig. 1. Schematics of diffusive vs. direct radiative transfer in an internally heated medium comprised of grains. In a low temperature gradient, each grain is effectively isothermal. The shades of the grains indicate the gradual temperature change. Diffusion (white arrows) involves emissions of photons by a hot grain, which are absorbed by nearby warm grains, which emit light in accord with their cooler temperatures. Each grain is both an emitter and a receiver. Black arrow denotes direct transfer of a photon from a hot to a cold grain: here, negligible interaction with the intervening grains occurs.

absorption coefficient that is independent of frequency which gives $k_{\rm rad} \propto T^3$ (e.g. Goto et al., 1980; Ross, 1997; Gibert et al., 2005). However, neither approach addresses the effect of grain-size. Two corrections are needed.

First, emissivity is an essential component of radiative transfer models used in engineering (Siegel and Howell, 1972; Brewster, 1992), astronomy (Evans, 1992; Kaufmann and Freedman, 2002), and remote sensing (Hapke, 1993). Based on these efforts to depict diverse situations involving radiative transfer, Section 2 revises the equations used in geophysics to include emissivity being frequency dependent. Second, scattering was neglected even though experiments show that scattering from grain boundaries shortens the photon's mean free path (Fujisawa et al., 1968). Finite interface reflection also increases opacity, especially at frequencies where absorbance is high. Section 2 accounts for both effects of physical scattering, which, when combined with emissivity, lead to a strong, non-linear relationship of $k_{\rm rad,dif}$ with grain-size.

Section 3 reports new IR spectra on olivine at elevated temperature, and combines these data with recent measurements of visible spectra at high T (Taran and Langer, 2001; Ullrich et al., 2002) for use in the model. Section 4 quantifies the complex dependence of $k_{\rm rad,dif}$ on T, d, and Fe^{2+} concentration. Geophysical implications are discussed in Section 5.

2. A semi-empirical model for calculation of diffusive radiative transfer

2.1. The current geophysical model, definitions, and assumptions

For local radiative equilibrium, optically thick conditions, and non-opaque media:

$$k_{\rm rad,dif}(T) = \frac{4\pi}{3}\int_0^\infty \Lambda(\nu, T)\frac{c}{\nu^2}\frac{\partial\{[n(\nu, T)]^2 S(\nu, T)\}}{\partial T}\,{\rm d}\nu. \quad (1)$$

where Λ is the mean free path, n the index of refraction, c the speed of light, ν frequency in $\rm cm^{-1}$, and T is the temperature. Clark (1957) and Shankland et al. (1979) presumed that the source function (S) is

Planck's blackbody function:

$$I_{\mathrm{bb}}(\nu) = \frac{2h\nu^5}{c^3}\left[\frac{1}{\exp(hc\nu/k_{\mathrm{B}}T) - 1}\right] \tag{2}$$

where h is the Planck's constant, k_{B} the Boltzman's constant, and the energy-density is provided on a per wavelength basis. These equations follow the conventions in geophysical literature except that $\nu = 1/\lambda$, as used in mineral spectroscopy, whereas Hofmeister (2004) used the convention of Brewster, which includes the factor of π in Eq. (2) rather than Eq. (1).

Radiative transfer involves two processes (absorption or physical scattering). Because their speeds are the same (=c), the mean free path is

$$\frac{1}{\Lambda} = \frac{1}{\Lambda_{\mathrm{attn}}} + \frac{1}{\Lambda_{\mathrm{scat}}} \tag{3}$$

(e.g. Lee and Kingery, 1960). For the weakly absorbing near-IR to UV regions, reflection and absorption are essentially independent phenomena. Material properties control both Λ_{attn} and Λ_{scat}, as follows.

Attenuation is related to the absorption coefficient:

$$A = -\frac{1}{z}\ln\left(\frac{I_{\mathrm{tra}}}{I_0}\right), \tag{4}$$

where I_{tra} is the transmitted intensity, I_0 the incident intensity, and z is thickness or the grain-size (Brewster, 1992). In mineralogy and chemistry, absorbance is computed from common logarithms [$a_{\mathrm{chem}} = -\log(I_{\mathrm{tra}}/I_0)$], but laboratory measurements of I_{tra} include not only losses from absorption, but also due to surface reflectivity (R). If internal scattering (e.g. due to fluid inclusions) is absent, the true absorbance (a) is

$$Az = 2.3026\,[a_{\mathrm{chem}} + 2\,\log(1 - R)] \tag{5}$$

(e.g. Shankland et al., 1979). For non-opaque minerals at normal incidence and for the weakly absorbing bands in the near-IR and visible spectral regions, $R = (n-1)^2/(n+1)^2$. Alternatively, baseline subtraction is used to obtain A from spectral measurements.

From Eq. (4), half the intensity is lost at a given frequency at a distance $z = 0.693/A(\nu)$. The mean free path is somewhat longer and has been approximated (e.g. Brewster, 1992) as

$$\Lambda_{\mathrm{attn}}(\nu) = 1/A(\nu). \tag{6}$$

Physical scattering has a directional dependence, but this is neglected since forward scattering dominates (Pitt and Tozer, 1970). The simple form suffices:

$$\Lambda_{\mathrm{scat}} = d \tag{7}$$

(Clark, 1957; Schatz and Simmons, 1972).

2.2. Why incorporate emissivity?

The previous geophysical model describes diffusion of blackbody radiation. Analogous equations in engineering texts (e.g. Brewster, 1992, Chapter 11, in particular, Fig. 11.1, pp. 369, 381, 385, also p. 228),

instead use the more realistic source function:

$$S(\nu, T) = \xi(\nu, T) I_{\rm bb}(\nu, T) \tag{8}$$

where ξ is the emissivity, a material property. For a greybody, ξ is <1 and independent of ν.

That emissivity is a component of $k_{\rm rad,dif}$ is confirmed with a thought experiment: consider removing one single grain from the mantle, which leaves a cavity with radius $r = d/2$. Vibrational transport into the vacant cavity is nil. The flux inside the cavity is $\xi\sigma T^4$, where $\sigma = 5.67\ {\rm W/m^2}$ is the Stefan-Boltzmann constant (e.g. Halliday and Resnick, 1966, p. 1175). From Carslaw and Jaeger (1960, p. 7):

$$-k_{\rm rad,dif}\frac{\partial T}{\partial r} = {\rm flux} = \xi\sigma T^4 \tag{9}$$

Thus, $k_{\rm rad,dif}$ must be proportional to ξ. Dimensional analysis provides an approximate solution:

$$k_{\rm rad,dif} \sim \xi\sigma T^3 r. \tag{10}$$

The result is essentially emissivity multiplied by Clark's formula [$k_{\rm rad} = (16/3)\sigma T^3 \Lambda$], because the mean free path is $\sim r$ for the non-absorbing cavity. Because Clark's result is obtained from Eq. (1) by replacing S with $I_{\rm bb}$ when Λ is constant, this analysis shows that Eq. (1) must include the factor ξ to represent radiative diffusion in a grainy medium.

In essence, emissivity is incorporated to comply with local radiative equilibrium for a grainy medium. That is, the light reaching any given grain essentially equals the light it emits.

Emissivity can be measured, but is generally obtained from absorption spectra using Kirchhoff's (circa 1869) law (e.g. Brewster, 1992; Molster et al., 2001; Kaufmann and Freedman, 2002). The simplest form of Kirchhoff's law is

$$\xi(\nu) = 1 - \exp[-dA(\nu)] \tag{11}$$

(e.g. Siegel and Howell, 1972; Hapke, 1993), where d is the thickness of the emitting layer or the grain-size of a particle, and A is from Eqs. (4) and (5). Kirchoff's law has been experimentally confirmed (Low and Coleman, 1966; Bates, 1978). The above references, Evans (1992), and Hofmeister et al. (2003) provide additional discussion of emissivity and grain-size.

2.3. Revision of the attenuation model for diffusive radiative transfer

The physical process in the mantle involves emission of light by each grain, which is diffused through partial absorption or scattering by neighboring particles (Fig. 1, white arrows). This semi-classical, macroscopic approach assumes that the particles emitting and absorbing light are of finite size, and that temperature is uniform within a single grain. Combining Eqs. (1), (3), (6)–(8) and (11):

$$k_{\rm rad,dif}(T) = \frac{4\pi}{3}\int_0^\infty \left(\frac{d}{1 + dA(\nu, T)}\right)\frac{c}{\nu^2}\frac{\partial}{\partial T}\left\{[n(\nu, T)]^2[1 - {\rm e}^{-dA(\nu,T)}] I_{\rm bb}(\nu, T)\right\}\,{\rm d}\nu \tag{12}$$

An average grain-size and emissivity is assumed to represent the medium, as in many radiative transfer models (e.g. Evans, 1992; Brewster, 1992). This assumption parallels use of an average grain-size to represent viscous damping in geodynamic models (e.g. Ranalli, 2001).

Given that radiative transfer models are approximate, I simplify Eq. (12) based on the dependence of material properties on ν, T, and P. The near-IR to UV spectral range need only be considered, as the

lattice modes in the far- to mid-IR, and the metal-oxygen charge transfer bands in the far-UV are too intense to permit radiative transfer.

The temperature and frequency dependence of n can be neglected. Based on density largely controlling n (e.g. the series $Mg_xFe_{2-x}SiO_4$: Bowen and Schairer, 1935), at ambient conditions $\partial n/\partial T$ is approximately:

$$\frac{\partial n}{\partial T} = -\alpha K_T \frac{\partial n}{\partial P} = -1.45 \times 10^{-6}\, K^{-1} \tag{13}$$

where P is the pressure, α the thermal expansivity ($2.66 \times 10^{-5}\,K^{-1}$: Suzuki, 1975), K_T the bulk modulus (127 GPa: Webb, 1989), and $\partial n/\partial P$ in the visible directionally averages to $0.00043\,GPa^{-1}$ for forsterite (Kirk and Vedam, 1972). The temperature derivative of n is very small and can be neglected. From the near-IR to UV, n depends weakly on ν (e.g. Wooten, 1972). Thus, n is placed outside the integral and approximated by its value in the visible.

Absorbance in the near-IR to UV regions changes strongly with temperature (Fig. 2), but $\xi(T)$ varyies only from 0 to 1 (Eq. (11)). The change in I with T overshadows that of ξ with T (Fig. 2). Thus, integration is performed over $\xi\partial I/\partial T$ rather than over $\partial(\xi I)/\partial T$.

A method is now developed to take scattering at the grain-boundaries into account in computing the attenuation of light. This step is necessary because the model is not valid for frequency regions where the grains are opaque (Clark, 1957). Such segments are excluded when integrating Eq. (12).

Opacity occurs when the product $dA(\nu)$ reaches a critical value such that the light from any given grain cannot reach its second nearest-neighbor. This critical value depends on R, the interface reflectivity, determined by the index of refraction mismatch through Snell's law ($n_2 \sin\theta_2 = n_1 \sin\theta_1$, where n_1 and n_2 are the indices of refraction for the two media and the corresponding angle, θ, is zero for normal incidence), and Fresnel's equations:

$$R_{\perp}^{1/2} = \frac{n_1 \cos\theta_1 - n_2 \cos\theta_2}{n_1 \cos\theta_1 + n_2 \cos\theta_2} \quad \text{and} \quad R_{\parallel}^{1/2} = \frac{n_1 \cos\theta_2 - n_2 \cos\theta_1}{n_1 \cos\theta_2 + n_2 \cos\theta_1}. \tag{14}$$

At normal incidence, $n_1 = 1.635$ and $n_2 = 1.670$ for two of the crystallographic axes in forsterite gives $R = 0.01\%$. At 45° incidence, $R_{\perp} = 0.04\%$ and $R_{\parallel} = 0\%$. At 60° incidence, $R_{\perp} = 0.16\%$ and $R_{\parallel} = 0.05\%$. As the angle becomes steeper, both R values increase to 100%. Similar values pertain to well-formed interfaces between olivine and other mantle minerals. A series of possible R values are investigated, as follows.

Including only the sections of the integral where $dA < 7$ ($R = 0.1\%$), corresponds to subhedral grain textures with ~120° angles, common in mantle rocks. This case is preferred as it is the most realistic. The case $dA < 10$ (i.e., where $R = 0.005\%$ prevents transmission beyond the distance d according to Eqs. (4) and (5)) corresponds to normal incidence which dominates textures in sheared rocks. The opacity limit $dA < 5$ ($R = 0.7\%$) depicts large grains which are difficult to fit together. The case $dA < 4$ ($R = 1.8\%$) may represent rough, angular textures.

Based on the above, Eq. (12) simplifies to

$$k_{\mathrm{rad,dif}}(T) = \frac{4\pi d n^2}{3} \sum \int_{\mathrm{lower}}^{\mathrm{upper}} \frac{1 - e^{-dA}}{(1 + dA)\,\nu^2} \frac{\partial[\, I_{\mathrm{bb}}(\nu, T)]}{\partial T}\, d\nu \tag{15}$$

where the sum allows for transparent regions existing above and below the strong bands in the visible. Because A is a complex function of ν (Fig. 2) and the cutoff frequencies depending on d and A, Eq. (15) is evaluated numerically.

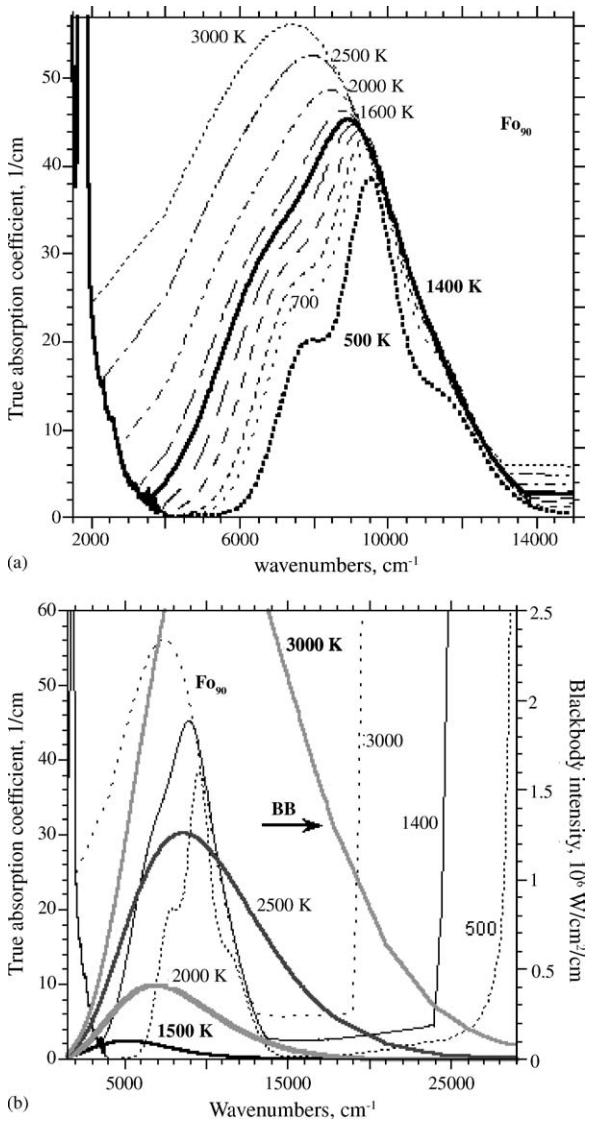

Fig. 2. Frequency dependent inputs for $k_{rad,dif}$. (a) Olivine absorption spectra. Contributions from surface reflections were subtracted from the raw data. Data below 4000 cm^{-1} were obtained from a 0.18 mm section, **E**‖**c**, of Fo_{90}. Data from 4000 to 15,000 cm^{-1} are fits provided by Taran and Langer (2001), averaged to remove orientation effects, doubled to represent mantle Fe^{2+} contents, and adjusted to match the spectra of Ullrich et al. (2002) at high temperature. The UV tail is modeled after the above studies. Heavy dots = 500 K; wide dots = 700 K; short dash = 800 K; medium dash = 1000 K; long dash = 1200 K; heavy solid = 1400 K; long-short dash = 1600 K; dot-dash = 2000 K; dot-dot-dash = 2500 K; fine dots = 3000 K. (b) Blackbody emission spectra (heavy lines), referring to right *y*-axis scale. Light lines = olivine spectra at 500, 1400, and 3000 K, pertaining to left *y*-axis scale. The position where the UV tail becomes steep was estimated from the results of Ullrich et al. (2002).

2.4. Asymptotic limits

Eq. (15) must be valid as A approaches zero, because physical scattering alone limits photon travel to the diffusive regime for low temperature gradients in the mantle. For largely transparent materials:

$$k_{\mathrm{rad,dif}}(T) \cong \frac{4\pi d^2 n^2}{3} \sum \int_{\mathrm{lower}}^{\mathrm{upper}} \frac{A}{\nu^2} \frac{\partial[\, I_{\mathrm{bb}}(\nu, T)]}{\partial T} \,\mathrm{d}\nu, \quad \text{for } dA \text{ small.} \tag{16}$$

As $A \to 0$, $k_{\mathrm{rad,dif}} \to 0$. No radiative transfer occurs because the energy from a photon cannot be converted into vibrations of the lattice without an absorbing mechanism. The case of no medium is properly represented because as $d \to 0$, $k_{\mathrm{rad,dif}} \to 0$. This situation can be viewed as the limit encountered for an ultra fine-grained ceramic.

If the product dA is very large (i.e., emissivity $\to$ 1), Eq. (15) reduces to Shankland et al. (1979) result:

$$k_{\mathrm{rad,dif}}(T) \cong \frac{4\pi n^2}{3} \sum \int_{\mathrm{lower}}^{\mathrm{upper}} \frac{1}{A\nu^2} \frac{\partial[I_{\mathrm{bb}}(\nu, T)]}{\partial T} \,\mathrm{d}\nu, \quad \text{for } dA \text{ large.} \tag{17}$$

For an opaque medium ($A \to \infty$) the correct limit ($k_{\mathrm{rad,dif}} \to 0$) is obtained. For very large d (when A is not miniscule) the grains are blackbodies, and $k_{\mathrm{rad,dif}} \to 0$. Thus, the new model provides the correct limits for end-member cases of the material properties. The formula of Shankland et al. (1979) is not valid for very weakly absorbing regions unless grain-size is large.

2.5. Pressure affects diffusive radiative transfer weakly

Because I_{bb} is independent of pressure (e.g. Sakurai, 1967), $k_{\mathrm{rad,dif}}(P)$ is controlled by the pressure dependence of the material properties. The index of refraction changes negligibly with P (see Eq. (13)). Spectra have not been measured at simultaneously high P and T, but the effect of P on $k_{\mathrm{rad,dif}}$ should be small because the peaks shift with pressure but maintain area and the integral is not terribly sensitive to position. That $\partial\nu/\partial P$ at 298 K is near or equal to zero for many absorption bands (e.g. Burns, 1982) further limits this effect. Once temperature is high enough that the absorption peak is contained within the blackbody curve (above ~1900 K, Fig. 2) then its shift with P is inconsequential and $\partial k_{\mathrm{rad,dif}}/\partial P$ can clearly be neglected. This temperature corresponds to the 670 km discontinuity (e.g. Ito and Takahashi, 1989). Thus, $\partial k_{\mathrm{rad,dif}}/\partial P$ is important only to the upper mantle and transition zone, where P is low.

3. Spectral values used to ascertain diffusive radiative transfer in the mantle

3.1. Experimental methods

Large, gem-quality crystals of olivine ($Mg_{1.8}Fe_{0.2}SiO_4$) from Spat, Nanga Parbat, Pakistan, were sawed along (0 1 0) and doubly polished to various thicknesses. Absorption spectra over frequencies of ~1800–8500 cm^{-1} were collected at 1 cm^{-1} resolution with an accuracy of ~0.01 cm^{-1} in a Fourier transform IR spectrometer (Bomem DA 3.02) using a SiC-globar source, a CaF_2 beamsplitter, an InSb detector, and a wire grid polarizer on a KRS-5 substrate. For the range ~500–4000 cm^{-1}, a KBr beamsplitter and an HgCdTe detector were used. Samples were heated to 673 K using a Spectratech heater with an Omega temperature controller after Gehring and Hofmeister (1994). Spectra were baseline subtracted.

3.2. Olivine spectra

Spectra used in the calculations are shown in Fig. 2. For $\nu < 4000\,cm^{-1}$, spectra were scaled for $\mathbf{E}\|\mathbf{c}$ from a thin crystal at 673 K. The other polarizations provide similar near-IR tails. Because the overtones near $1700\,cm^{-1}$ control the IR tail and their frequency shift compensates for their broadening, use of the 673 K spectrum is valid over temperature. The small contribution of the overtone region to $k_{rad,dif}$ further justifies this approximation.

For $\nu > 4000\,cm^{-1}$, peaks due to d–d transitions of Fe^{2+} in olivines with 5, 10 and 100% fayalite component (Taran and Langer, 2001; Ullrich et al., 2002) shift to lower frequencies as T increases. The central, strong peak near $9200\,cm^{-1}$ decreases in intensity, whereas the two weak bands ($\nu \sim 8000$ and $11000\,cm^{-1}$) increase in intensity. The new measurements show that the change in peak area is small, in contrast to previous data of Shankland et al. (1979). Earlier studies exist but have been discounted due to problems with oxidation (Shankland et al., 1979). The above near-IR data confirm that A from 4000 to $6000\,cm^{-1}$ negligibly increases up to 673 K, as seen by Taran and Langer (2001) and Ullrich et al. (2002). Comparing the spectra at 1273 K of Ullrich et al. (2002) to that of Shankland et al. (1979), shows that the earlier study had an underlying baseline that grew with temperature, and is not considered further.

To construct a directionally averaged average spectrum, the fit of Taran and Langer (2001) was initially used to provide visible spectra for Fo_{90} for T up to 3000 K. The linear fit parameters produced more intensity than that measured by Ullrich et al. (2002) at the highest temperatures, so curvature was added to the fit to reproduce the later data at 1273 K.

A UV tail like that of Taran and Langer (2001) was appended, as this sample has the least Fe^{3+}. As temperature increases, the UV bands increase and shift downwards. The rise in A just above the Fe^{2+} bands (Fig. 2) was estimated using data from Ullrich et al. (2002). Weak, spin-forbidden Fe^{2+} bands superimposed on the UV tail contribute negligibly to $k_{rad,dif}$. For Fo_0Fa_{100}, the UV tail at 273 K rises steeply at $25{,}000\,cm^{-1}$ whereas at 1273 K the rise begins at $20{,}000\,cm^{-1}$. For $Fo_{95}Fa_5$, the UV rise onsets at $30{,}000\,cm^{-1}$ at 298 K. The projection (Fig. 2b), based on comparing these data, underestimates the curvature in A with ν. Evaluating the uncertainties at high temperature (Section 3) takes this underestimate into account.

Cutoff frequencies for Eq. (15) are listed for the lowest value of R (0.005%, corresponding to the opacity limit $dA < 10$): For $d = 0.01$ cm, the integral is over $1000–36{,}000\,cm^{-1}$. For $d = 0.1$ cm, the integral is evaluated from 1770 to $28{,}000\,cm^{-1}$. When $d = 1$ cm and for temperatures below 1000 K, the ranges are $2500–7000\,cm^{-1}$, and $12{,}500–20{,}000\,cm^{-1}$. Higher absorbance at T of 1200–1600 K suggests the narrower interval of $2500–5000\,cm^{-1}$, whereas by 2500 K, olivine is opaque in all the near-IR. For $d = 10$ cm, the integral is evaluated over 3600–6000 and $13{,}000–20{,}000\,cm^{-1}$ if $T < 800$ K, but over $3600–4400\,cm^{-1}$ for $1000 < T < 1600$ K. For $d = 100$ cm, olivine is opaque at all temperatures and all frequencies, and $k_{rad,dif}$ is 0.

For the three other R values considered, the limits of integration were determined from Fig. 2 at each temperature examined. The temperature at which each given grain-size becomes opaque at all frequencies was also estimated, to provide a constraint at high T.

3.3. Why olivine is used to represent the mantle

Optical spectra at high temperature or at UV frequencies are lacking for many deep mantle phases. For this reason, olivine is used as model compound for the mantle. This approximation is reasonable because dense phases share many spectral features, and integration should smooth over spectral details.

Lattice overtone spectra are similar for all silicates. Overtones for oxides (e.g. MgO) occur at lower frequency because the fundamentals occur at low ν (e.g. Hofmeister et al., 2003), and thus the lower limit in Eq. (15) would be reduced. Because the near-IR region contributes little to $k_{rad,dif}$ and silicates should constitute more than 80% of the mantle, olivine reasonably depicts the overtone region.

The strength and position of the main, spin-allowed band of Fe^{2+} strongly affects $k_{rad,dif}$. Due to the similarities of their sites, absorption spectra for olivine strongly resemble those of pyroxene (Burns, 1970), magnesiowüstite (Goto et al., 1980), and wadsleyite (Ross, 1997). Electronic transitions in ringwoodite should be similar to those in olivine, because the spectrum of γ-Fe_2SiO_4 closely resembles the directionally averaged spectra of fayalite (cf. Mao and Bell, 1972; Ullrich et al., 2002). The spin-forbidden bands and the UV tails of these diverse mantle materials are also similar. For these materials, our results for $k_{rad,dif}$ should be accurate, especially insofar as radiative transfer models are approximate.

For other mantle phases, using olivine spectra to approximate $k_{rad,dif}$ is a reasonable first approximation because peak parameters vary little for main Fe^{2+} band. For all of the phases listed above as well as (Mg,Fe)SiO_3 perovskite (Keppler et al., 1994) and majorite (Ross, 1997), $A \sim 16$ cm and $\nu \sim 9000\,cm^{-1}$ for Fe/(Mg + Fe) ~ 0.1. However, deep mantle phases have bands not present in olivine that can affect $k_{rad,dif}$.

Garnets have an additional band near $5000\,cm^{-1}$. Spectra of majorite and pyrope are virtually the same, even for pyrope with negligible Fe^{3+}, and assignment of $\sim$4500 cm^{-1} band in pyrope to electronic transitions of Fe^{2+} is long-standing (e.g. Manning, 1967). Bands near $5000\,cm^{-1}$ in majorite are thus due to d–d transitions of Fe^{2+} in a rather large structural site. Because these bands are weak and at low frequency, their effect on $k_{rad,dif}$ is probably small and limited to low T (cf. Fig. 2b).

Perovskite (Keppler et al., 1994) has an extra band near $14{,}000\,cm^{-1}$. However, strong physical scattering exists above $\sim$10,000 cm^{-1}, and thus values of A in the visible are uncertain, and the UV region is unconstrained. The likely effect of the second band of perovskite on $k_{rad,dif}$ is discussed below.

Spectra are unavailable for the post-perovskite phase (ppv), which is stable at conditions in the deepest mantle. Since ppv has a site for Fe similar to that of perovskite (high coordination number, distorted, and large: Murakami et al., 2004), these two phases will have similar $k_{rad,dif}$.

Spectra are unavailable for low spin Fe^{2+}. If A is low as surmised by Badro et al. (2004), then Eq. (16) is valid and $k_{rad,dif}$ is small and largely dependent on grain size.

In the mantle, Fe^{3+} is present in low quantities. Radiative transfer is negligibly affected because bands due to electronic transitions of Fe^{3+} are not only weak and narrow, but are superimposed on the strong, broad Fe^{2+} bands or the UV tail (see e.g. Ullrich et al., 2002).

4. Results

Eq. (15) was evaluated numerically using the above input parameters. Using d from 0.01 to 100 cm reveals the grain-size dependence. Using the preferred $R = 0.1\%$ and three other values accounts for variations in surface reflectivity that arise from texture. Results are presented for olivine with Fe/(Mg + Fe) = 0.1, and the effect of varying the Fe^{2+} content is discussed.

4.1. Temperature dependence of $k_{rad,dif}$ for Fe/(Mg+Fe) of 0.1

Radiative transfer is a complex function of T, d, and R (Fig. 3). Only for small ($\leq$mm) grain-sizes, is $k_{rad,dif}(T)$ simple, that is, a quadratic polynomial suffices (Table 1).

Table 1
Analytical forms for $k_{rad,dif}$ shown in Figs. 3 and 4

Grain size (cm)	Temperature range (K)	Least squares fit W/m K with T in K
Scattering 0.005%		
0.01	500–6000	$0.055522 - 0.00013855T + 8.6603 \times 10^{-8}T^2$
0.1	500–6000	$0.40399 - 0.0011265T + 8.6069 \times 10^{-7}T^2$
0.5	500–2500	$-1.415 + 0.011522T - 3.4484 \times 10^{-5}T^2 + 4.7507 \times 10^{-8}T^3 - 3.0432 \times 10^{-11}T^4 + 9.0177 \times 10^{-15}T^5 + 9.9754 \times 10^{-19}T^6$
0.5	2000–9700[a]	$19.855 - 0.022552T + 8.875 \times 10^{-6}T^2 - 1.1879 \times 10^{-9}T^3 + 5.061 \times 10^{-14}T^4$
0.5	2500–6000	$-6.34 + 0.00348T$
1	500–2500	$-14.156 + 0.08349T - 0.00019249T^2 + 2.1958 \times 10^{-7}T^3 - 1.274 \times 10^{-10}T^4 + 3.58223 \times 10^{-14}T^5 - 3.8552 \times 10^{-18}T^6$
1	2000–4700[a]	$175.2 - 0.24325T + 0.00012013T^2 - 2.4659 \times 10^{-8}T^3 + 1.7923 \times 10^{-12}T^4$
10	500–2000[a]	$25.329 - 0.13596T + 0.00025642T^2 - 1.9815 \times 10^{-7}T^3 + 5.3666 \times 10^{-11}T^4$
Scattering 0.1%[b]		
0.01	500–6000	$0.055368 - 0.00013839T + 8.6605 \times 10^{-8}T^2$
0.1	500–6000	$0.36776 - 0.0010594T + 8.3496 \times 10^{-7}T^2$
0.5	500–6000[a]	$6.7171 - 0.031439T + 5.1615 \times 10^{-5}T^2 - 3.688 \times 10^{-8}T^3 + 1.2664 \times 10^{-11}T^4 - 1.9998 \times 10^{-15}T^5 + 1.1634 \times 10^{-19}T^6$
1	500–2350	$-2.0395 + 0.021162T - 7.2869 \times 10^{-5}T^2 + 1.1137 \times 10^{-7}T^3 - 7.9913 \times 10^{-11}T^4 + 2.6645 \times 10^{-14}T^5 - 3.3311 \times 10^{-18}T^6$
1	700–3250[a]	$8.8147 - 0.042611T + 7.1949 \times 10^{-5}T^2 - 5.1634 \times 10^{-8}T^3 + 1.6446 \times 10^{-11}T^4 - 1.8946 \times 10^{-15}T^5$
5	500–1400[a]	$2.0021 - 0.0119808T + 2.042 \times 10^{-5}T^2 - 9.2494 \times 10^{-9}T^3$
10	500–1200[a]	$0.049595 - 0.0068702T + 1.93 \times 10^{-5}T^2 - 1.135 \times 10^{-8}T^3$
Scattering 0.7%		
0.01	500–6000	$0.051455 - 0.00013144T + 8.4016 \times 10^{-8}T^2$
0.1	500–6000	$0.047183 - 0.00041778T + 5.6185 \times 10^{-7}T^2$
0.5	700–5000[a]	$6.4801 - 0.030518T + 5.1001 \times 10^{-5}T^2 - 3.7773 \times 10^{-8}T^3 + 1.3632 \times 10^{-11}T^4 - 2.2931 \times 10^{-15}T^5 + 1.4329 \times 10^{-19}T^6$
1	700–2600[a]	$66.406 - 0.41253T + 0.010334T^2 - 1.3669 \times 10^{-6}T^3 + 1.0428 \times 10^{-9}T^4 - 4.6072 \times 10^{-13}T^5 + 1.0926 \times 10^{-16}T^6 - 1.0734 \times 10^{-20}T^7$
5	500–1200[a]	$10.762 - 0.049486T + 7.1957 \times 10^{-5}T^2 - 3.1827 \times 10^{-8}T^3$
Scattering 1.8%		
0.01	500–6000	$0.05185 - 0.00013192T + 8.4054 \times 10^{-8}T^2$
0.1	500–6000	$0.12791 - 0.00045686T + 4.7883 \times 10^{-7}T^2$
0.5	500–3000	$-2.6228 + 0.018764T - 5.1485 \times 10^{-5}T^2 + 6.7454 \times 10^{-8}T^3 - 4.2996 \times 10^{-11}T^4 + 1.2889 \times 10^{-14}T^5 - 1.4473 \times 10^{-18}T^6$
0.5	1400–3800[a]	$16.013 - 0.075775T + 0.00013068T^2 - 1.0461 \times 10^{-7}T^3 + 4.193 \times 10^{-11}T^4 - 8.0773 \times 10^{-15}T^5 + 5.9198 \times 10^{-19}T^6$
1	500–2100[a]	$-22.434 + 0.1474T - 0.00038353T^2 + 5.0152 \times 10^{-7}T^3 - 3.4426 \times 10^{-10}T^4 + 1.182 \times 10^{-13}T^5 - 1.6002 \times 10^{-17}T^6$
5	500–1200[a]	$4.5947 - 0.022802T + 3.546 \times 10^{-5}T^2 - 1.6378 \times 10^{-8}T^3$

Values of $k_{rad,dif} = 0$ for $d = 100$ cm for $R = 0.005$ and 0.1%, and $k_{rad,dif} = 0$ for $d = 10$ for 0.1 and 1.8%. The uncertainties in the fits increase with temperature above 2000 K.

[a] At higher T, $k_{rad,dif} = 0$.

[b] Preferred parameterization corresponding to equi-granular textures found in the mantle. For $d = 1$ cm, the lower temperature fit better matches the calculations, but extrapolating to high temperature is not reliable.

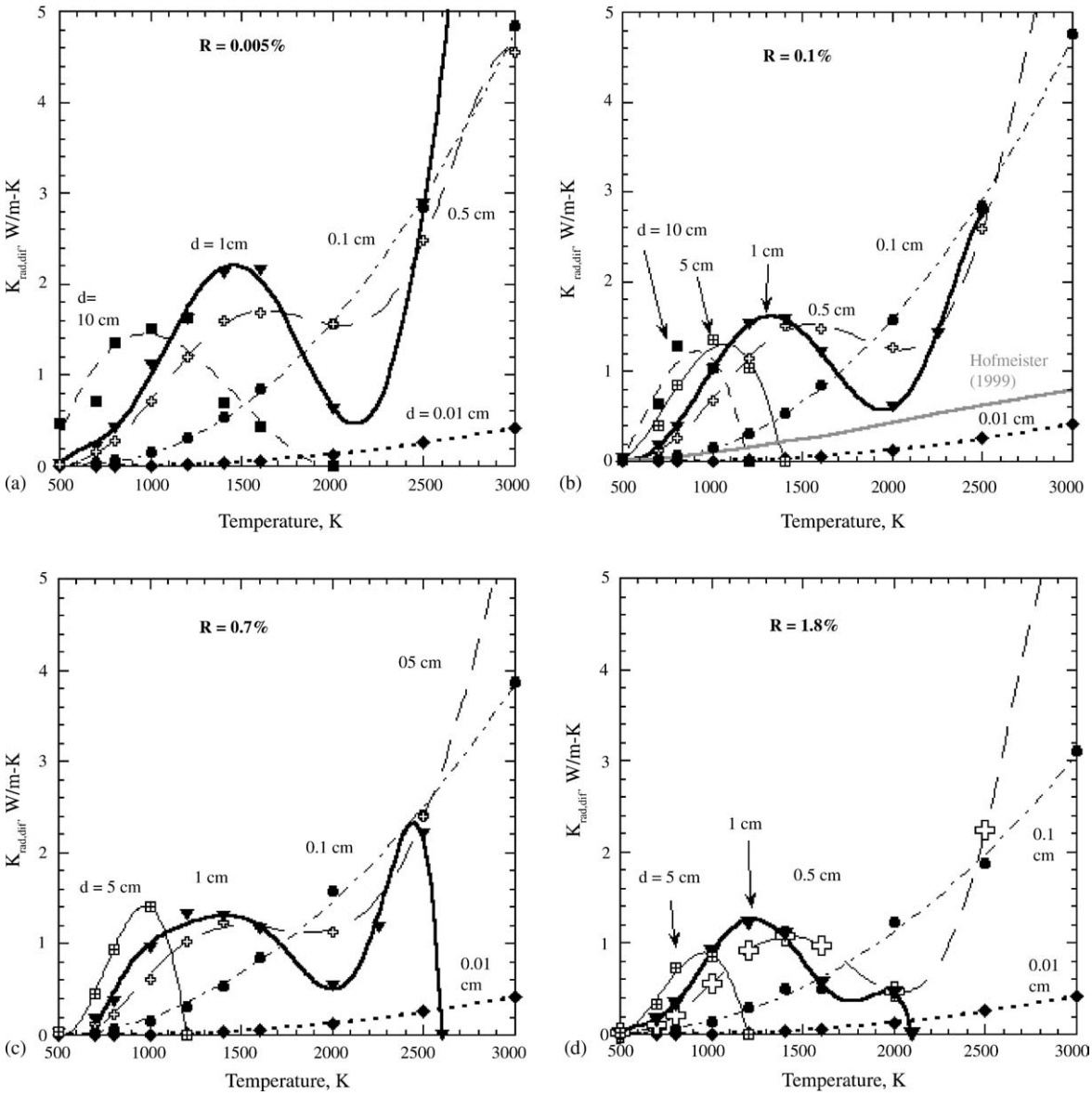

Fig. 3. Temperature dependence of $k_{rad,dif}$ for olivine. Symbols are the calculated values. Curves are polynomial fits (Table 1). Diamonds and dotted curve for grain-size of 0.01 cm. Circles and dot-dashed curve: $d = 0.1$ cm. Open cross and long dash curve: $d = 0.5$ cm. Triangles and heavy solid line: $d = 1$ cm. Square with cross and light solid line; $d = 5$ cm. Squares and dashed line: $d = 10$ cm. Grey curve = parameterization of Hofmeister (1999): (a) calculations assuming that opacity occurs for $dA \geq 10$, (b) opacity occurring for $dA \geq 7$, (c) opacity occurring for $dA \geq 5$, and (d) opacity occurring for $dA \geq 4$.

For moderate grain-sizes (several mm to 1 cm), $k_{rad,dif}(T)$ has local maxima and minima (Fig. 3). A hill-and-valley profile exists because the blackbody peak increases in frequency as T increases, and thus is convoluted with different spectral regions as T rises (Fig. 2a), each of which have different amounts of absorption (Fig. 2a) leading to strong variation in $k_{rad,dif}(T)$. The maximum in $k_{rad,dif}$ at low temperature is

related to the near-IR "window" wherein radiative transfer is promoted, as discussed by Shankland et al. (1979), but requires large grain size, so that Eq. (17) is valid. The second maximum at high temperature is due to an analogous window in the UV (Fig. 2), and requires moderate grain sizes since A becomes larger as temperature increases and because the product dA is the important quantity. The minimum exists near 2000 K because at this temperature, the blackbody curve coincides with the envelope of the Fe^{2+} bands (Fig. 2b). In essence, radiative transfer is inhibited in the absorbing visible region relative to the efficient transmitting regions on either side of the Fe^{2+} peak. For perovskite, the additional band in the visible should reduce the hill and valley effect.

For large d (∼cm), a cubic polynomial describes the single maximum (Fig. 3), which results from the highest transmissions occurring in the near-IR. As grain-size decreases, the local and global maxima shift to higher temperature, reaching well above 3000 K for $d < \sim 3$ mm.

Similar trends are seen in $k_{\mathrm{rad,dif}}$ (T) for all values of R. But, as reflectivity at the grain-boundaries increases, the grains become opaque over larger spectral regions, and $k_{\mathrm{rad,dif}}$ decreases overall (Fig. 3). Huge grains become particularly ineffective at radiative transport. For moderate grain-sizes, varying R impacts the form of $k_{\mathrm{rad,dif}}$ (T), e.g. the hills and valleys are pronounced for 0.5 cm grains, but diminished for others (Fig. 3). For $d = 1$ cm, as R increases, a second maximum develops at high T for and then shrinks. For small grains, R little impacts $k_{\mathrm{rad,dif}}$.

For $T \geq 2500$ K, the results (Fig. 3) are approximate mostly because the UV region is estimated. The uncertainty in $k_{\mathrm{rad,dif}}$ at high T depends on grain-size. (1) Large grain-sizes do not participate in radiative transfer at high temperature, and are not affected. (2) For $d \leq 1$ mm, whether A changes gradually or abruptly at high ν negligibly changes the already low A values. The quadratic fits for small d (Table 1) should be valid at mantle conditions. (3) Intermediate grain-sizes have large uncertainties in $k_{\mathrm{rad,dif}}$ at high T, which depend on R. The development of a small second maximum for $d = 1$ cm at $R = 0.7\%$ (Fig. 3c), which becomes even smaller as scattering increases (Fig. 3d) suggests that $k_{\mathrm{rad,dif}}$ is overestimated for $d = 1$ cm at high T for low R (Fig. 3a and b). However, for $d = 0.5$ cm, $k_{\mathrm{rad,dif}}$ is constrained at very low R (Fig. 3a) because grains this size transmit over all frequencies. In this case, the form used for UV tail is unimportant.

To compensate for approximating the UV tail as rising abruptly (Fig. 2b), rather than gradually, values for $k_{\mathrm{rad,dif}}$ used in Fig. 3 are reduced by 5% at 2500 K and by 10% at 3000 K for the rest of the paper. Although this adjustment for "curvature" is rough, the resulting values for $k_{\mathrm{rad,dif}}$ are more realistic at high temperature, and are included in deriving the fits of Table 1.

To further constrain $k_{\mathrm{rad,dif}}$, I used Fig. 2 to estimate the temperature where the UV region absorbs enough to quench radiative transfer, i.e., T where $k_{\mathrm{rad,dif}} = 0$. Null point temperatures less than 4000 K are fairly certain, resulting in well-constrained curves (Fig. 4; Table 1). Achieving model accuracy above 2500 K for all d and R, requires higher temperature data at UV frequencies, a difficult experimental task.

4.2. Grain-size dependence of $k_{rad,dif}$ for Fe/(Mg + Fe) of 0.1

If $d = 0$, or if $A = 0$ over all frequencies, $k_{\mathrm{rad,dif}} = 0$ (Eqs. (15) and (16)). Because light is back reflected at interfaces, grains are opaque when the transmitting region reaches some high A-value, which depends on d and R, and $k_{\mathrm{rad,dif}}$ is again zero. This size is ∼100 cm for $Fo_{90}Fa_{10}$ with minimal interface reflectivity and ∼10 cm for large R (Fig. 3; Table 1). Thus, radiative transfer at a given temperature should increase with d at small d, reach a maximum and then decrease. Because I_{bb} increases with temperature, $k_{\mathrm{rad,dif}}$ at a

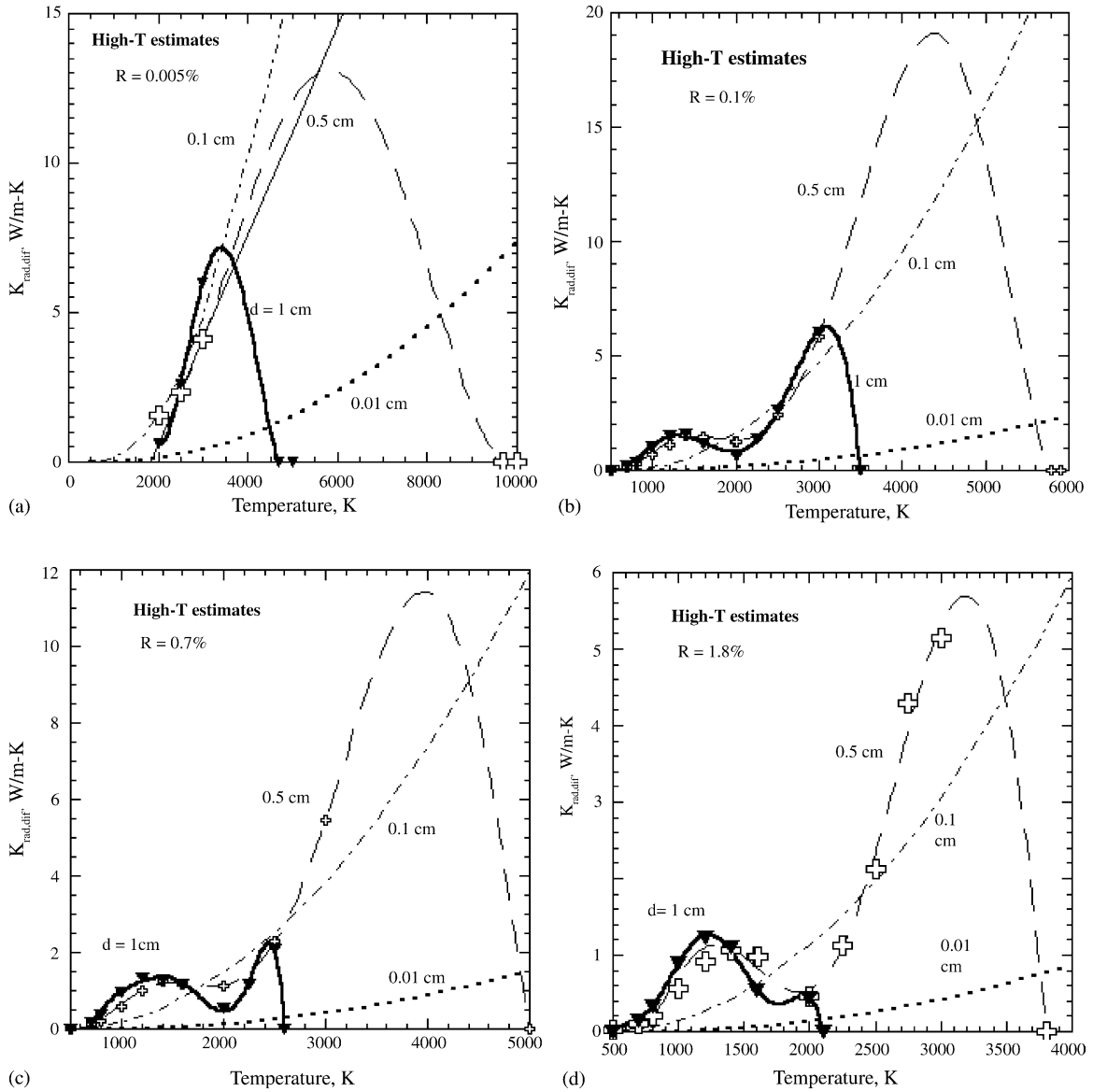

Fig. 4. High-temperature extrapolations for olivine. Symbols as in Fig. 3; fits as in Table 1.

given grain-size should generally increase with T. The calculations provide these expected characteristics (Fig. 5).

For low R, $d = 10$ cm provides the largest $k_{rad,dif}$ at low temperature (Fig. 5a and b). Grain-size near 1 cm is most effective at moderate temperatures, shifting to $d \sim 0.5$ cm near 1800 K, and at high temperature, $d \sim 0.1$ cm produces high $k_{rad,dif}$. The development of a second maximum in $k_{rad,dif}$ near d of 1 cm as T passes 2500 K is questionable because the high T result depends on the particulars of UV tail: $k_{rad,dif}$ at high T is uncertain for this grain-size.

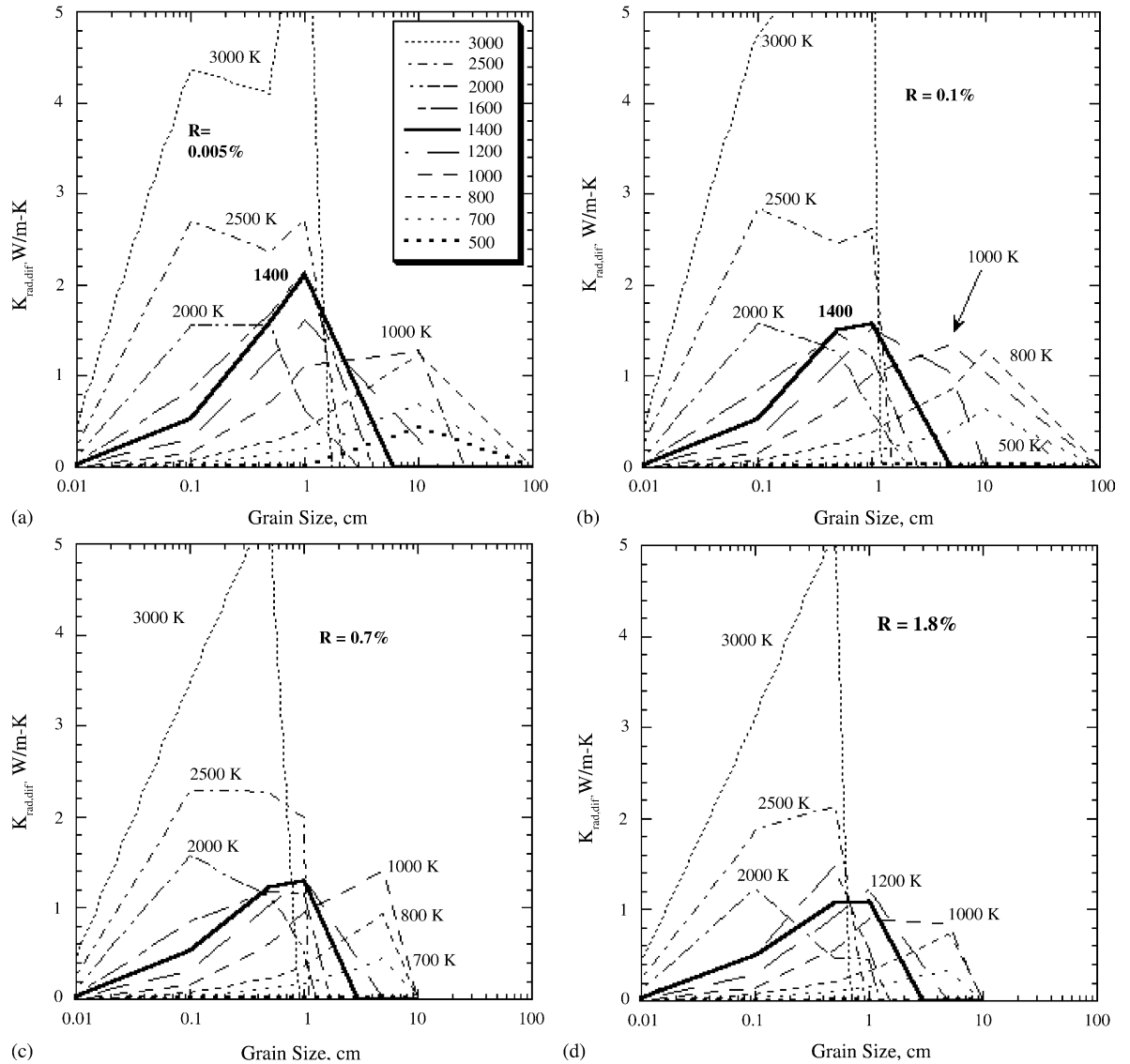

Fig. 5. Grain-size dependence of $k_{rad,dif}$ for olivine. Legend (inset in part a) is the same as in Fig. 2 and subsequently: (a) calculations assuming that opacity occurs for $dA \geq 10$, (b) opacity occurring for $dA \geq 7$, (c) opacity occurring for $dA \geq 5$, and (d) opacity occurring for $dA \geq 4$. In part (a), the curve for $d = 1$ cm seem overestimated at high T, whereas in parts (b–d), the curves for $d = 0.5$ cm seem overestimated at high T, see text.

4.3. Effect of interface reflectivity

From geometric considerations, interface reflectivity of 0.1% is expected for equi-granular textures of mantle rocks. This case provides the preferred values and is shown in part (b) of Figs. 3–5 and listed in Table 1. For sheared textures, $R \sim 0.01\%$: The results shown in part (a) of Figs. 3–5 provide an upper

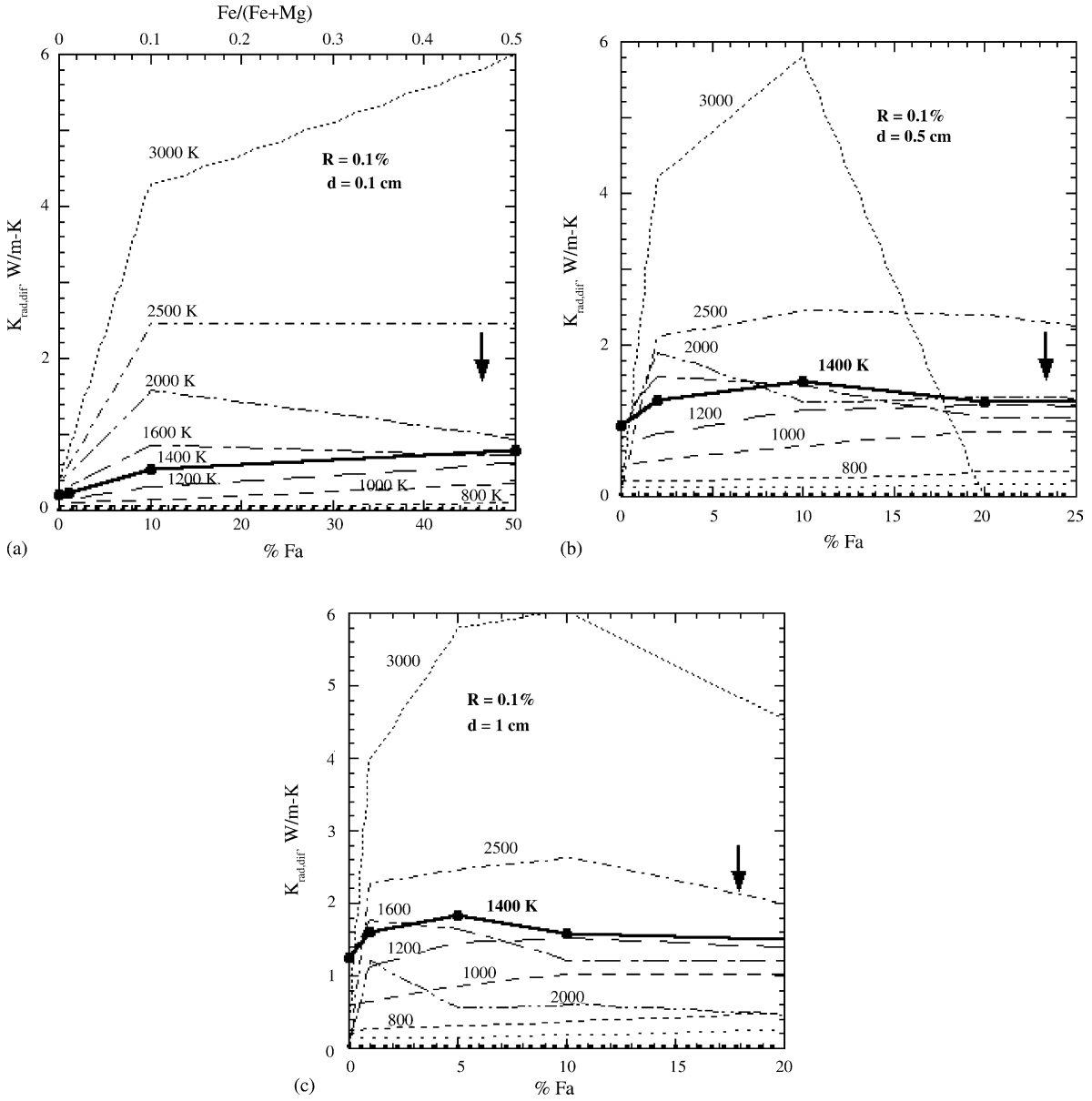

Fig. 6. Dependence of $k_{rad,dif}$ on Fe content in olivine. Symbols as in Fig. 4. Opacity is assumed to occur for $dA \geq 7$ (the preferred case): (a) grain-size of 0.1 cm, (b) grain-size of 0.5 cm, and (c) grain-size of 1 cm. The arrow shows that the results are overestimated at $T > 2500$ K and high Fe content. At constant grain-size, as T increases the maximum shifts to lower Fe contents. At constant T, as grain-size increases, the maximum shifts to lower Fe content. Increasing scattering also moves the minimum to lower Fe content.

limit. The main effect of increasing R at any given temperature is to shift the maxima in $k_{rad,dif}$ in d towards smaller grain sizes (Fig. 5). As R increases, $k_{rad,dif}(d)$ is reduced, but this effect is not large.

4.4. Effect of Fe^{2+} content on $k_{rad,dif}$

From Beer's law, A is proportional to the concentration of the entity producing the bands (e.g. Rossman, 1988). This linear relationship exists between Fe^{2+} content and the strengths of the electronic bands from 0 to 100% fayalite (Taran and Langer, 2001; Ullrich et al., 2002). The relevant quantity in Eq. (13) is dfX where f is the Beer's law proportionality constant, and X is the Fe^{2+} content. From this proportionality, $k_{rad,dif}(T)$ for Fa_{10} when $d = 1$ cm is equivalent to $k_{rad,dif}(T)$ for Fa_{20} with $d = 0.5$ cm, ignoring momentarily the contribution of the overtones, and that the UV tail shifts toward the visible as Fe content increases. I therefore subtracted the contribution below 4000 cm^{-1} from the results for Fa_{10}, used proportionality relationships to determine the contribution of the Fe bands as a function of Fe^{2+} content, and summed this result with the overtone region for the appropriate grain-size to provide $k_{rad,dif}(T, d, X)$. Neglecting the shift of the UV tail with Fe overestimates $k_{rad,dif}$ for samples with >10% Fa above ~2200 K.

At low temperatures, high Fe content enhances $k_{rad,dif}$ slightly (Fig. 6), consistent with band tails in the near-IR being the controlling factor. For upper mantle temperatures, maxima exist in $k_{rad,dif}$ as a function of Fe^{2+} content, as expected, by analogy to Fig. 5. For constant d and R, the Fe^{2+} content of the maximum initially decreases as temperature increases, remaining constant between ~1500 and ~2200 K, and moving to higher Fe content as T increases further (Fig. 6). The shift in the maximum at high temperature to high Fe^{2+} content clearly results from overestimation of $k_{rad,dif}$ due to the uncertainty in extrapolating the UV region. The positions of the maxima at 1600–2000 K should represent the behavior of $k_{rad,dif}$ at higher T.

Increasing d moves the maxiumum in $k_{rad,dif}$ to lower Fe contents when T and R are held constant (as in Fig. 6). Increasing R sharpens the maximum in $k_{rad,dif}(Fe^{2+})$ and the lower temperature curves are affected more(not shown).

For narrow O–H stretching bands, the effect of concentration of the absorbing entity was extracted from Eq. (15) using the trapezoid rule (Hofmeister, 2004). A functionally similar dependence on X was observed.

5. Conclusions and geophysical implications

5.1. General behavior

The above calculations use olivine spectra and an average grain size to approximate diffusive radiative transport in an anhydrous, ferrous, silicate-rich, multi-phase mantle with idealized interface reflectivities. The precise values of $k_{rad,dif}$ will diverge from these approximations, as the mantle has multiple phases and a grain-size distribution, but integration is a smoothing function, which reduces the importance of spectral details. Results for small-grain size are the least dependent on the spectra, and should hold for all other phases with high-spin Fe^{2+}. For large grain-size, the results depict upper mantle phases (olivine, pyroxene and spinel). The local maximum should be subdued for perovskite and garnet phases with their broader absorption bands. The following results should be generally applicable.

Radiative transfer depends strongly and non-linearly on grain-size. The dependence of $k_{rad,dif}$ on d is determined by two competing effects. For frequencies where $A(\nu)$ is large, increasing d means that larger parts of the integral become negligible, which reduces $k_{rad,dif}$. This effect competes non-linearly with $k_{rad,dif}$ being proportional to d^2 for transparent regions (Eq. (16)).

Trends in $k_{rad,dif}$ with T are complex because the controlling variables (absorbance, opacity limits, blackbody intensity) depend non-linearly on temperature. Only if A is independent of both T and of ν, is $k_{rad,dif}$ proportional to T^3, which is the commonly assumed form (e.g. Clark, 1957). As temperature increases, d giving the highest $k_{rad,dif}$ decreases. Importantly, the change in sign of $\partial k_{rad,dif}/\partial T$ from positive to negative occurs at higher T as d decreases such that for grain-sizes $<\sim$0.1 cm, $\partial k_{rad,dif}/\partial T$ is positive for all possible mantle temperatures.

The dependence of absorbance on Fe^{2+} content allows inference of the compositional dependence of $k_{rad,dif}$. Because $k_{rad,dif}$ depends on the product dA and has maxima for certain d values, it must also have a maximum at a particular Fe^{2+} content. The calculations indicate that optimal radiative transport occurs for Fe/(Mg + Fe) $\sim$0.1 at mantle temperatures for $d \sim$ 0.1–0.2 cm, or near Fe/(Mg + Fe) $\sim$0.02 for $d \sim$ 0.5–1 cm.

5.2. Comparison with previous models and the phonon contribution

The present results for most grain-sizes are considerably larger than those of Hofmeister (1999), which compare closely to the present model with $d = 0.02$ cm and $R = 0.1\%$ (Fig. 3b). Results of Shankland et al. (1979) resemble the curve for $d = 1$ cm up to 1300 K, but continue rising to 2 W/m K at 1600 K. Calculations were not performed above this temperature, but the trend suggests a weak dependence on temperature at high T. The previous models thus correspond to small and large grains found in mantle rocks (e.g. Boyd and Meyer, 1979).

The lattice component is roughly 5 W/m K at ambient temperature, and decreases monotonically to about 2.5 W/m K near 1500 K, and is flat thereafter (see summary by Hofmeister, 1999; Hofmeister and Yuen, 2005). For the upper mantle, the lattice component dominates heat transfer for small grains, whereas both phonon and photon contributions are important for large and moderate grains.

5.3. Connection of mantle grain-size and layering with $k_{rad,dif}$

Grain-size critically affects rheology in the mantle (Riedel and Karato, 1997). This dependence leads to a non-linear response to strain and heating (Kameyama et al., 1997; Braun et al., 1999), and, thus, viscosity is considered to be important in earth's thermal history (e.g. Tozer, 1965; Stacey and Loper, 1988). Similarly, a grain-size dependence for heat transport properties must have repercussions for mantle dynamics.

The existence of maxima in the dependence of $k_{rad,dif}$ on d, T, and composition are especially important. Positive $\partial k/\partial T$ promotes stability in the mantle through positive feedback, and a negative derivative is destabilizing, causing more erratic, vigorous convection (Dubuffet et al., 2002). The different signs for the derivative above and below $\sim$2000 K at moderate grain-size, the correspondence of $T \sim$ 2000 K with the major seismic discontinuity at 670 km (Ito and Takahashi, 1989), and the evolution of the system towards both stability and efficient heat transport, suggest that different styles of convection could exist for the shallow and deep mantle. To explore this further, we discuss the available constraints on grain-size.

The combination of efficient radiative diffusion and viscous shear suggests a small grain-size in the lower mantle, ∼0.1 cm. This size has positive $\partial k/\partial T$, and provides large values of $k_{\rm rad,dif}$ above ∼2000 K. Lower mantle rheology is not well constrained (Ranalli, 2001), but d has been estimated from mantle viscosity as 0.3 cm near 670 km (Yamazaki and Karato, 2001), which is compatible with the present result. This upper mantle differs: d varies from 0.01 to 1 cm, such that individual samples have a range of grain sizes (e.g. Boyd and Meyer, 1979). For lower temperatures in the upper mantle, the model presented here suggests that larger grains are better at transporting heat via photons. However, at such lower temperatures, phonons transport significant amounts of the heat as well (e.g. Hofmeister, 1999).

The upper and lower mantle layers differ substantially in grain-size, in rheology, in the relative proportion of heat transported by phonons or by photons, and in the sign of $\partial k/\partial T$. These differences point towards layered convection.

5.4. Continuous parameterization of $k_{rad,dif}$ with T and d for dynamic models

Geodynamic models exploring the evolution of grain size have utilized a continuous parameterization of viscosity on d. Applying the same approach to radiative transfer may yield further information on the time-dependence of mantle convection. The non-linear dependence of $k_{\rm rad,dif}$ on d and T precludes reduction to one formula. But, a continuous parameterization can be provided for the three distinct regimes of small, moderate, and large grain-size. Gaussians and polynomials are used to approximate the results for $R = 0.1\%$ (Fig. 4b):

$$k_{\rm rad,dif} = 10d[0.36776 - 0.0010594T + 8.3496T^2], \quad \text{for } d < 0.2\,\text{cm} \tag{18}$$

$$k_{\rm rad,dif}(d,T) = [5 + 22(1-d)]\exp\left[\frac{-[T - 2800 - 2600(1-d)]^2}{[400 + 1400(1-d)]^2}\right] + [1.7 - 0.2(1-d)]\exp\left[\frac{-[T - 1400 - 300(1-d)]^2}{[500 + 200(1-d)]^2}\right], \quad 0.2 < d < 1.2\,\text{cm} \tag{19}$$

and

$$k_{\rm rad,dif}(d,T) = [1.35 + 0.03(10-d)]\exp\left[\frac{-[T - 900 - 6(10-d)^2]^2}{[230 + 2(10-d)^2]^2}\right], \quad 1 < d < 100\,\text{cm} \tag{20}$$

5.5. Fe-rich silicates and the deepest mantle

High Fe content in O-rich phases decreases both $k_{\rm lat}$ (Horai, 1971; Hofmeister, 2001; Giesting and Hofmeister, 2002) and $k_{\rm rad,dif}$ for high spin Fe^{2+} in olivine. All other phases will behave similarly although the maxima would occur at different X and d. Low spin Fe^{2+} should weakly absorb visible and UV light and will have a smaller value of $k_{\rm rad,dif}$ at any given temperatures compared to the corresponding high spin state at low Fe contents (Eq. (16)). As Fe content increases, the UV tail grows and thus for some large X, A is large and Eq. (17) holds. Optimal radiative transport for low spin Fe thus exists but at higher

Fe contents and grain size than for the high spin configuration. Thus, for an oxide mineralogy, the layer above the core (D'') has lower k_{tot} and would be destabilized through large amounts of Fe^{2+} enrichment (discussed further by Hofmeister and Yuen, 2005).

Radiative transfer in sulfides such FeS (troilite) differ in important ways. From reflectivity (Peckett, 1992) and IR absorption measurements (Hofmeister et al., 2003), FeS has large A that is independent of frequency. For such a greybody, Clark (1957) formula, modified to account for emissivity and grain-size, is valid:

$$k_{\text{grey}} = \frac{16}{3}\xi n^2 \sigma T^3 \left(\frac{d}{1+dA}\right) \tag{21}$$

Depending on tradeoffs between the value of A (which is large, but unknown in the visible, requiring quantitative analysis of spectral reflectance), and on the grain size, radiative transfer in a deepest mantle that is dominated by metal-sulfides could be huge due to the T^3 response.

Acknowledgements

I thank Dave Yuen, Jeremy Yates, Angela Speck, Bob Criss, and Janet Bowey for enlightening discussions, and W.A. Bassett and Arie van den Berg for helpful reviews. M.N. Taran kindly shared spectra of olivine at temperature. Support was provided by NSF-EAR-0125883.

References

Badro, J., Rueff, J.-P., Vanko, G., Monoco, G., Fiquet, G., Guyot, F., 2004. Electronic transition in perovskite: possible non-convecting layers in the lower mantle. Science 305, 383–386.

Bates, J.B., 1978. Infrared emission spectroscopy. Fourier Transform IR Spectr. 1, 99–142.

Bowen, N.L., Schairer, J.F., 1935. The system MgO–FeO–SiO_2. Am. J. Sci. 24, 177–197.

Boyd, F.R., Meyer, H.O.A., 1979. The mantle sample: inclusions in kimberlites and other volcanics. In: Proceedings of the Second International Kimberlite Conference, vol. 2, American Geophysical Union, Washington, DC, p. 424.

Braun, J., Chery, J., Poliakov, A.N.B., Mainprice, D., Vauchez, A., Tomassi, A., Daignieres, M., 1999. A simple parameterization of strain localization in the ductile regime due to grain-size reduction: a case study for olivine. J. Geophys. Res. 104, 25167–25181.

Brewster, M.Q., 1992. Thermal Radiative Transfer and Properties. John Wiley & Sons Inc., New York.

Burns, R.G., 1970. Mineralogical Applications of Crystal Field Theory. Cambridge University Press, Oxford.

Burns, R.G., 1982. Electronic spectra of minerals at high pressures: how the mantle excites electrons. In: Schreyer, W. (Ed.), High-pressure Researches in Geoscience. E. Schweizerbartsche Verlag, Stuttgart, pp. 223–246.

Carslaw, H.S., Jaeger, J.C., 1960. Conduction of Heat in Solids. Clarendon Press, Oxford.

Clark Jr., S.P., 1957. Radiative transfer in the earth's mantle. Trans. Am. Geophys. Union 38, 931–938.

Dubuffet, F., Yuen, D.A., Rabinowicz, M., 1999. Effects of a realistic mantle thermal conductivity on the patterns of 3-d convection. Earth Planet. Sci. Lett. 171, 401–409.

Dubuffet, F., Yuen, D.A., Rainey, E.S.G., 2002. Controlling thermal chaos in the mantle by positive feedback from radiative thermal conductivity. Nonlinear Proc. Geophys. 9, 1–13.

Evans, A., 1992. The Dusty Universe. Ellis Horwood, New York.

Fujisawa, H., Fujii, N., Mizutani, H., Kanamori, H., Akimoto, S., 1968. Thermal diffusivity of Mg_2SiO_4, Fe_2SiO_4, and NaCl at high pressures and temperatures. J. Geophys. Res. 75, 4727–4733.

Gehring, A.U., Hofmeister, A.M., 1994. The transformation of lepidocriocite during heating: a magnetic and spectroscopic study. Clays Clay Miner. 42, 409–415.

Gibert, B., Schilling, F.R., Tommasi, A., Mainprice, D., 2003. Thermal diffusivity of olivine single-crystals and polycrystalline aggregates at ambient condition – a comparison. Geophys. Res. Lett. 30 (22), 2172, doi:10.1029/2003GL018459.

Gibert, B., Schilling, F.R., Gratz, K., Tommasi, A., 2005. Thermal diffusivity of olivine single crystals and a dunite at high temperature. Evidence for heat transfer by radiation in the upper mantle. Phys. Earth Planet Int. 151, 129–141.

Giesting, P.A., Hofmeister, A.M., 2002. Thermal conductivity of disordered garnets from infrared spectroscopy. Phys. Rev. B 65, #144305 (15 pages).

Goto, T., Ahrens, T.J., Rossman, G.R., Syono, Y., 1980. Absorption spectrum of shock-compressed Fe^{2+}-bearing MgO and the radiative conductivity of the lower mantle. Phys. Earth Planet. Int. 22, 277–288.

Halliday, D., Resnick, R., 1966. Physics. John Wiley & Sons, New York.

Hapke, B., 1993. Theory of Reflectance and Emittance Spectroscopy. Cambridge University Press, Cambridge.

Hofmeister, A.M., 1999. Mantle values of thermal conductivity and the geotherm from photon lifetimes. Science 283, 1699–1706.

Hofmeister, A.M., 2001. Thermal conductivity of spinels and olivines from vibrational spectroscopy at ambient conditions. Am. Miner. 86, 1188–1208.

Hofmeister, A.M., 2004. Enhancement of radiative transfer in the mantle by OH^- in minerals. Phys. Earth Planet. Int. 146, 483–485.

Hofmeister, A.M., Yuen, D.A., 2005. The threshold dependencies of thermal conductivity and implications on mantle dynamics. Earth Planets Space, submitted for publication.

Hofmeister, A.M., Keppel, E., Speck, A.K., 2003. Absorption and reflection infrared spectra of MgO and other diatomic compounds. Mon. Not. R. Astron. Soc. 345, 16–38.

Horai, K., 1971. Thermal conductivity of rock-forming minerals. J. Geophys. Res. 76, 1278–1308.

Ito, E., Takahashi, E., 1989. Postspinel transitions in the system Mg_2SiO_4–Fe_2SiO_4 and some geophysical implications. J. Geophys. Res. 94, 10637–10646.

Kameyama, M., Yuen, D.A., Fujimoto, H., 1997. The interaction of viscous heating with grain-size dependent rheology in the formation of localized slip zones. Geophys. Res. Lett. 24, 2523–2526.

Kanamori, H., Fujii, N., Mizutani, H., 1968. Thermal diffusivity measurement of rock-forming minerals from 300 to 1100 K. J. Geophys. Res. 73, 595–603.

Kaufmann, R., Freedman, W.J., 2002. Universe. W.H. Freeman, New York.

Keppler, H., McCammon, C.A., Rubie, D.C., 1994. Crystal-field and charge-transfer spectra of $(Mg,Fe)SiO_3$ perovskite. Am. Miner. 79, 1215–1218.

Kirk, J.L., Vedam, K., 1972. Piezo-optic behavior of forsterite Mg_2SiO_4. J. Phys. Chem. Solids 33, 1251–1255.

Lee, D.W., Kingery, W.D., 1960. Radiation energy transfer and thermal conductivity of ceramic oxides. J. Am. Ceram. Soc. 43, 594–607.

Low, M.J.D., Coleman, I., 1966. Measurement of the spectral emission of infrared radiation of minerals and rocks using multiple-scan interferometry. Appl. Opt. 5, 1453–1455.

Manning, P.G., 1967. The optical absorption spectra of the garnets almandine-pyrope, pyrope and spessartine and some structural interpretations of mineralogical significance. Can. Miner. 9, 237–251.

Mao, H.K., Bell, P.M., 1972. Optical and electrical behavior of olivine and spinel (Fe_2SiO_4) at high pressure. Carnegie Inst. Wash. Yr. Bk. 71, 520–524.

Mehling, H., Huatzinger, G., Nilsson, O., Fricke, J., Hofmann, R., Hahn, O., 1998. Thermal diffusivity of semitransparent materials determined by the laser-flash method applying a new analytical model. Int. J. Thermophys. 19, 941–949.

Molster, F.J., Lim, T.L., Sylvester, R.J., Waters, L.B.F.M., Barlow, M.J., Beintema, D.A., Cohen, M., Cox, P., Schmitt, B., 2001. The complete ISO spectrum of NGC-6302. Astron. Astrophys. 372, 165–172.

Murakami, M., Hirose, K., Kawamura, K., Sata, N., Ohishi, Y., 2004. Post-perovskite phase transition in $MgSiO_3$. Science 306, 855–858.

Peckett, A., 1992. The Colours of Opaque Minerals. Van Nostrand Reinhold, New York.

Pitt, G.D., Tozer, D.C., 1970. Radiative heat transfer in dense media and its magnitude in olivines and some other ferromagnesian minerals under typical upper mantle conditions. Phys. Earth Planet Int. 2, 189–199.

Ranalli, G., 2001. Mantle rheology: radial and lateral viscosity variations inferred from microphysical creep laws. J. Geodyn. 32, 425–444.

Riedel, M.R., Karato, S., 1997. Grain-size evolution in subducted oceanic lithosphere associated with the olivine-spinel transformation and its effects on rheology. Earth Planet Sci. Lett. 148, 27–44.

Ross, N.L., 1997. Optical absorption spectra of transition zone minerals and implications from radiative heat transfer. Phys. Chem. Earth 22, 113–118.
Rossman, G.R., 1988. Optical spectroscopy. Rev. Miner. 18, 207–254.
Sakurai, J.J., 1967. Advanced Quantum Mechanics. Addison-Wesley Publishing Company Inc., Reading, Massachusetts.
Schatz, J.F., Simmons, G., 1972. Thermal conductivity of earth materials at high temperature. J. Geophys. Res. 77, 6966–6983.
Shankland, T.J., Nitsan, U., Duba, A.G., 1979. Optical absorption and radiative heat transport in olivine at high temperature. J. Geophys. Res. 84, 1603–1610.
Siegel, R., Howell, J.R., 1972. Thermal Radiation Heat Transfer. McGraw-Hill, New York.
Stacey, F.D., Loper, D.E., 1988. Thermal history of the Earth: a corollary concerning non-linear mantle rheology. Phys. Earth Planet Int. 53, 167–174.
Suzuki, I., 1975. Thermal expansion of periclase and olivine and their anharmonic properties. J. Phys. Earth 23, 145–149.
Taran, M.N., Langer, K., 2001. Electronic absorption spectra of Fe^{2+} ions in oxygen-based rock-forming minerals at temperatures between 297 and 600 K. Phys. Chem. Miner. 28, 199–210.
Tozer, D., 1965. Heat transfer and convection currents. Phil. Trans. R. Soc. London A 258, 252–271.
Ullrich, K., Langer, K., Becker, K.D., 2002. Temperature dependence of the polarized electronic absorption spectra of olivines. Part I. Fayalite. Phys. Chem. Miner. 29, 409–419.
van den Berg, A.P., Yuen, D.A., Steinbach, V.C., 2001. The effects of variable thermal conductivity on mantle heat-transfer. Geophys. Res. Lett. 28, 875–878.
van den Berg, A.P., Yuen, D.A., Rainey, E.S.G., 2004. The influence of variable viscosity on delayed cooling due to variable thermal conductivity. Phys. Earth Planet Int. 142, 283–295.
Webb, S.L., 1989. The elasticity of the upper mantle orthosilicates olivine and garnet to 3 GPa. Phys. Chem. Miner. 16, 684–692.
Wooten, F., 1972. Optical Properties of Solids. Academic Press Inc., San Diego.
Yamazaki, D., Karato, S.I., 2001. Some mineral physics constraints on the rheology and geothermal structure of earth's lower mantle. Am. Miner. 86, 385–391.
Yanagawa, T.K.B., Nakada, M., Yuen, D.A., 2005. The influence of lattice thermal conductivity on thermal convection with strongly temperature-dependent viscosity. Earth Space Sci. 57, 15–28.
Yuen, D.A., Vincent, A.P., Bergeron, S.Y., Dubuffet, F., Ten, A.A., Steinbach, V.C., Starin, L., 2000. Crossing of scales and nonlinearities in geophysical processes. In: Boschi, E., Ekstrom, G., Morelli, A. (Eds.), Problems in Geophysics for the New Millenium. Editrice Compositori, Bologna, Italy, pp. 405–465.